Risk-Aware Security-Constrained Unit Commitment

Daniel Bienstock, Yury Dvorkin, Cheng Guo, Robert Mieth, Jiayi Wang

***Abstract*—To better handle real-time load and wind generation volatility in unit commitment, we present an enhancement to the computation of security-constrained unit commitment (SCUC) problem. More specifically, we propose a two-stage optimization model for SCUC, which aims to provide a risk-aware schedule for power generation. Our model features a data-driven uncertainty set based on principal component analysis, which accommodates both load and wind production volatility and captures locational correlation of uncertain data. To solve the model more efficiently, we develop a decomposition algorithm that can handle nonconvex subproblems. Our extensive experiments on NYISO dataset show that the risk-aware model protects the public from potential high costs caused by adverse circumstances.**

***Index Terms*—Security-constrained unit commitment, wind uncertainty, data-driven uncertainty set.**

I. Introduction

In wholesale electricity markets, Security Constrained Unit Commitment (SCUC) computations are crucial for day-ahead scheduling of power generation [1]. The day-ahead schedule is corrected via the Reliability Unit Commitment (RUC) process [2], which is roughly similar to SCUC but is closer to the actual power delivery and, thus, has more accurate forecast information. Finally, in real time, a dispatch computation (a linear program) is used to determine generator output within the next short-term time window (typically, 5-15 minutes). Both SCUC and RUC are deterministic computations and currently use single-point estimates of load averages for each specific hourly or half-hourly period; real-time dispatch, on the other hand, relies on firm estimates of *average* loads in the ensuing time window. Significant load or generation deviations within the real-time window are handled via reserves, which are set up as exogenous reserve requirements. This combination of prediction-driven scheduling and real-time correction has proved successful and represents a strong engineering accomplishment.

However, forthcoming large-scale deployment of renewable generation, as well as battery resources and controllable loads, challenges this paradigm. In particular, renewables may, under adverse circumstances, introduce large and structured real-time deviations from expected generation levels – this is termed below as *volatility*. It is worth noting that even high-quality and probabilistic forecasts cannot bypass volatility, which is a reflection of real-time stochasticity. As a result, providing additional reserve to compensate for this volatility may increase the operating cost, partially or fully offsetting the economic advantage of zero-marginal renewable generation. Since some ISOs (e.g., NYISO) co-optimize energy and reserves [3], the combined cost incurred by the energy and reserve provision is ultimately optimized and borne by the public. Moreover, this total cost is, clearly, a stochastic quantity, and high-cost excursions, if frequently observed, could become of interest to regulatory and government entities.

This paper presents an algorithmic enhancement to the SCUC and RUC computations that makes them risk-aware, or more precisely, volatility-aware, with the goal of yielding unit commitment (UC) decisions that are more robust to real-time load and generation volatility in terms of operational security *and* electricity pricing.

In this paper we specifically focus on financial and physical risks raised by critical time periods characterized by sharp load and/or renewable volatility. A pertinent example is provided by peak hours on high-load, high-variability or otherwise stressed days, which, as a result may experience very high discrepancy between real-time and day-ahead prices. See, for example, Figure 17 of [4] and Figure 3-7 of [5]. Empirical evidence (see, e.g. in [6, 7]) suggests that, additionally, virtual traders can forecast these periods quite accurately.

Our approach explicitly internalizes real-time price formation under adversarial conditions in the UC process and, using a real-world New York Independent System Operator (NYISO) dataset, demonstrates the beneficial impact of the proposed methodoloy on overall consumer cost.

A. Literature Review

The ubiquitous deployment of volatile energy resources has previously motivated numerous proposals to improve upon currently static reserve requirements and deterministic point forecasts through alternative probabilistic models [8, 9]. The UC process lends itself to being formulated as a two-stage stochastic program (SP) and has been proposed as such originally to tackle demand uncertainty [10, 11] and volatile renewable generation [12–16]. These approaches optimize the expected system cost of UC (first stage) and economic dispatch (second stage), and model uncertainty through scenarios or an estimated probability distribution. A popular alternative to SP-based approaches, avoiding their often prohibitive computational complexity and scenario requirements [13], is adaptive robust optimization (ARO) [17, 18]. This approach is a variant of robust optimization [19]. ARO models minimize day-ahead UC and real-time dispatch cost for a worst-case, real-time realization drawn from a pre-defined uncertainty set. For a given uncertainty set, this approach is computationally efficient and does not require the estimation or assumption of a specific underlying probability distribution. The uncertainty set itself can be estimated from data, but requires careful tuning to achieve good quality solutions that are not overly conservative [20]. Polyhedral sets as in [17, 18] are easy to implement but do not capture correlation information. As a result, variations could be overestimated, which leads to conservative, and thus more expensive, decisions. Various data-driven methods to create uncertainty sets for UC problems that avoid this shortcoming are discussed in [21].

All approaches [10–18, 21] minimize the total commitment and generation costs. However, the expected consumer cost resulting from extreme real-time price spikes is ignored. In this work, we propose a two-stage risk-aware optimization model for the SCUC problem that explicitly models both SCUC and real-time operations with a focus on consumer cost. We solve this model using a customized cutting plane-based algorithm. Inspired by factor stressing used in the financial services industry [22], we construct a data-driven uncertainty set based on principal component analysis (PCA) [23] to capture locational correlation, which models the stochasticity in both load and wind generation more realistically. While the constructed uncertainty set is similar to [24] (as used for UC in [21]), it is different in structure and adapted for our proposed SCUC model. To demonstrate our model on a real-world, large-scale NYISO case study, we also develop heuristics to reformulate the uncertainty set.

We summarize our contributions as follows:

- Inspired by how the mean-variance portfolio optimization problem [25] is made risk-aware, we add a volatility-dependent penalty term to the SCUC objective that reflects uncertainty in (real-time) consumer cost during a period of the day that is expected to be particularly risky (e.g., peak hours on a high-load day). Thus, our day-ahead model is made aware of an observed real-world phenomenon, namely real-time price spikes.
- We account for volatility by constructing adverse scenarios based on stressing factors. More specifically, we build a data-driven uncertainty set via PCA, with principal components obtained from real-world NYISO historical data. The uncertainty set captures locational correlation of uncertainty data, which include both load and wind generation.
- We develop an algorithm to solve the proposed nonconvex, risk-aware optimization model. The algorithm is similar to the Benders' decomposition scheme [26] and it iteratively refines a relaxed day-ahead problem by adding cuts generated from the adverse real-time problem. Due to nonconvex subproblems, our algorithm cannot directly adopt Benders cuts as have been done in [17] and [18]. Instead, we use no-good cuts [27], integer L-shaped cuts [28], and novel problem-specific logic-based Benders decomposition (LBBD) cuts [29]. We also speed up the algorithm by developing a grid search heuristic for the nonconvex real-time problem, and adding cuts via a branch-and-cut scheme. With the proposed solution approach, we are able to solve the large-scale NYISO case study efficiently.

II. Two-Stage Risk-Aware Optimization Model

Our modified SCUC computation builds on current industry practice [3] by extending common model formulations [1, 30] to incorporate expected volatility in real-time operations. Under such conditions, a financial penalty may ensue, and, possibly, actual physical risk may occur. Empirical evidence from virtual trader activity suggests that on selected periods of the year (e.g., high temperature days) high-volatility periods are predicted in advance [31].

To handle both financial and physical risk, while maintaining its overall structure, we modify the *objective* of the SCUC mixed-integer program (MIP) by adding a term that approximates volatility (i.e., risk) in the real-time financial cost during the time period of interest. Thus, the financial risk accounted for in our SCUC is a measure of consumer's real-time costs under load and renewable output forecast errors. The algorithmic implementation of this updated SCUC can be viewed as a two-stage model, where in the first stage a standard SCUC problem is addressed, and in the second stage the obtained solution is exposed to an appropriately instrumented adversary, which computes a realistic scenario for the critical time period that stresses a given SCUC solution. This stress computation relies on data-driven models of volatility in loads and wind power. The information gleaned from this process is incorporated, in appropriate form, into a revised SCUC computation which includes new constraints as well as an objective term that models the real-time financial risk. This cycle is repeated until a desirable convergence is attained. Figure 1 illustrates the relationship between the two stages of the model. The model in Figure 1 has two critical features. First, it does not depart from the standard SCUC paradigm in that it produces precisely the same output as SCUC does, namely, a UC decision. That UC decision can thus be used to obtain day-ahead locaitonal marginal prices (LMPs) [32] via the dual of the demand constraint, as done in practice via the so-called "pricing run". Second, our algorithm does not simply amount to a robust optimization approach in the sense that the objective function is a blend of day-ahead costs and real-time robustified costs, with the importance assigned to the second term controlled by a multiplier that reflects risk tolerance.

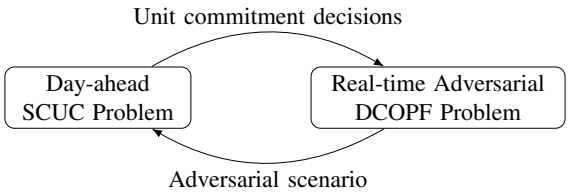

Fig. 1: Two-stage risk-aware optimization model

A. Model for Risk-Aware SCUC Problem

The proposed SCUC assumes the viewpoint of the system operator. In our model for the day-ahead market, we minimize the total cost of electricity production and generator start-up and shutdown, plus an estimate of the consumer cost attained in the real-time market, which are due to incorrect wind and/or load forecasts. The consumer cost is the payment incurred by the consumers in the real-time market when load is underestimated in the day-ahead market. Note that the consumer cost is, at the point of time when SCUC is run, an uncertain quantity.

In the formulation below, an *appropriately robust* estimate of the consumer cost is indicated by the quantity $\hat{V}$, which appears in the objective function (1) and in constraint (9e). Note that in the objective function $\hat{V}$ is scaled by a certain

weight $\rho > 0$ and the model becomes more risk-aware as ρ increases. Hence, we model the total cost as follows:

$$\sum_{t\in\mathcal{T}^{\mathrm{DA}}}\Big(\sum_{g\in\mathcal{G}}\big(h_{gt}+C_g^{\mathrm{Start}}v_{gt}+C_g^{\mathrm{Down}}w_{gt}\big) + \sum_{i\in\mathcal{N}}C^{\mathrm{VOLL}}p_{it}^{\mathrm{Unmet}}\Big)+\rho\hat{V}, \tag{1}$$

where the first four terms denote the production cost h_{gt}, startup cost C_g^{Start}, shutdown cost C_g^{Down}, and day-ahead value of lost load (VOLL) C^{VOLL}. In addition, $\mathcal{T}^{\mathrm{DA}}$ is the set of time periods (hours) in the day-ahead market, $\mathcal{G}$ is the set of generators, $\mathcal{N}$ is the set of buses. Binary variables v_{gt} and w_{gt} denote startup and shutdown decisions, and p_{it}^{Unmet} is the unsatisfied load. Note that h_{gt} is a piecewise linear function of power output p_{gt}, and can be modelled with constraints in (2). Each linear piece ($o \in \mathcal{O}$) in the piecewise linear function is represented by one constraint ($\forall t \in \mathcal{T}^{\mathrm{DA}}$):

$$h_{gt} \geq C_{og}^1 p_{gt} + C_{og}^0 y_{gt} \qquad \forall o\in\mathcal{O}, g\in\mathcal{G}^{\mathrm{Ther}}, \tag{2}$$

where binary variable y_{gt} denotes the commitment decision, C_{og}^1 and C_{og}^0 are respectively the slope and intercept for the cost segment o in the piecewise linear function, and $\mathcal{G}^{\mathrm{Ther}}$ is the set of thermal generators.

In addition, we have the following constraints in the day-ahead problem:

(1) *Load Constraints* ($\forall t \in \mathcal{T}^{\mathrm{DA}}$)*:* For each hour the day-ahead expected load $\bar{D}_{it}$ at each node is either satisfied by production at the node and power transmitted to the node, or by shedding load penalized by the VOLL. The set $\mathcal{G}_i$ includes both thermal and renewable (wind) generators at bus i, $\mathcal{L}$ is the set of transmission lines, and f_{ijt} is the power flow.

$$\sum_{g\in\mathcal{G}_i} p_{gt} + p_{it}^{\mathrm{Unmet}} + \sum_{(j,i)\in\mathcal{L}} f_{jit} - \sum_{(i,j)\in\mathcal{L}} f_{ijt} = \bar{D}_{it} \qquad \forall i\in\mathcal{N} \tag{3a}$$

$$p_{it}^{\mathrm{Unmet}} \geq 0 \qquad \forall i\in\mathcal{N}. \tag{3b}$$

(2) *Linearized (DC) Power Flow Constraints* ($\forall t \in \mathcal{T}^{\mathrm{DA}}$)*:* Constraint (4a) defines the linearized (DC) power flow in terms of the voltage angle difference $\theta_{it}-\theta_{ji}$ at time t between buses i and j and line susceptance B_{ij}. Constraints (4b) and (4c) bound flows.

$$f_{ijt} = B_{ij}\left(\theta_{it}-\theta_{jt}\right) \qquad \forall (i,j)\in\mathcal{L} \tag{4a}$$

$$f_{ijt} \leq P_{ij}^{\mathrm{Trans}} \qquad \forall (i,j)\in\mathcal{L} \tag{4b}$$

$$f_{ijt} \geq -P_{ij}^{\mathrm{Trans}} \qquad \forall (i,j)\in\mathcal{L}. \tag{4c}$$

(3) *Startup/Shutdown Decisions*: The following constraints link on/off statuses with startup and shutdown decisions.

$$v_{gt}-w_{gt} = y_{gt}-y_{g,t-1} \qquad \forall g\in\mathcal{G}^{\mathrm{Ther}}, t\in\mathcal{T}^{\mathrm{DA}}\setminus\{1\} \tag{5a}$$

$$v_{gt}, w_{gt}, y_{gt} \in \{0,1\} \qquad \forall g\in\mathcal{G}^{\mathrm{Ther}}, t\in\mathcal{T}^{\mathrm{DA}}. \tag{5b}$$

(4) *Production Constraints* ($\forall t \in \mathcal{T}^{\mathrm{DA}}$)*:* Constraints (6a) and (6b) set bounds for power outputs of thermal generator g. Constraints (6c) set the outputs of wind generator g at no more than $\bar{P}_{gt}^{\max}$, where $p_{gt}^{\mathrm{Curtail}}$ is the curtailed output, and $\mathcal{G}^{\mathrm{Wind}}$ is the set of wind generators.

$$p_{gt} \leq P_g^{\max} y_{gt} \qquad \forall g\in\mathcal{G}^{\mathrm{Ther}} \tag{6a}$$

$$p_{gt} \geq P_g^{\min} y_{gt} \qquad \forall g\in\mathcal{G}^{\mathrm{Ther}} \tag{6b}$$

$$p_{gt} + p_{gt}^{\mathrm{Curtail}} = \bar{P}_{gt}^{\max} \qquad \forall g\in\mathcal{G}^{\mathrm{Wind}} \tag{6c}$$

$$p_{gt} \geq 0 \qquad \forall g\in\mathcal{G} \tag{6d}$$

$$p_{gt}^{\mathrm{Curtail}} \geq 0 \qquad \forall g\in\mathcal{G}^{\mathrm{Wind}}. \tag{6e}$$

(5) *Ramping Constraints* ($\forall t \in \mathcal{T}^{\mathrm{DA}}\setminus\{1\}$)*:* The following constraints enforce generator multi-period ramping limit M_g.

$$p_{gt} - p_{g,t-1} \leq M_g y_{g,t-1} + P_g^{\min} v_{gt} \qquad \forall g\in\mathcal{G}^{\mathrm{Ther}} \tag{7a}$$

$$p_{g,t-1} - p_{gt} \leq M_g y_{gt} + P_g^{\min} w_{gt} \qquad \forall g\in\mathcal{G}^{\mathrm{Ther}} \tag{7b}$$

(6) *Risk-Aware Consumer Cost Model:* Lastly, we address the consumer cost paid in real-time. As described above we focus, in particular, on a critical and impactful set of time periods $\mathcal{T}^{\mathrm{RT}}$ which is *expected* to have high load and wind generation volatility. We assume that such time periods can be forecasted with significant certainty at the time of the SCUC computation – as stated above, empirical evidence suggests that this capability already exists. Our model provides a robust estimate for the real-time consumer cost during these critical time periods, taking into account the volatility of load and wind generation. More specifically, if the load at some bus i and time t is higher in real-time than anticipated in the first-stage, then the consumer needs to procure the difference at its real-time LMP. However, there is no real-time penalty for overestimating load in the first stage. More precisely, suppose that $\boldsymbol{\omega}$ indicates a *realization* of all quantities that are uncertain at the day-ahead phase, and known in real-time, including in particular the vector d_{it}^{RT} of real-time loads. Let $\lambda_{it}(\mathbf{y},\boldsymbol{\omega})$ be the corresponding real-time LMP, where the notation stresses the dependence on the unit-commitment vector $\mathbf{y}$ and the uncertain quantities $\boldsymbol{\omega}$. Then the consumer cost averaged over the number of time periods per hour in the critical time period $\mathcal{T}^{\mathrm{RT}}$, given realization $\boldsymbol{\omega}$, is given by the following expression:

$$V = V(\mathbf{y},\boldsymbol{\omega}) = \frac{1}{N^{\mathrm{tp}}}\sum_{t\in\mathcal{T}^{\mathrm{RT}}}\sum_{i\in\mathcal{N}}\lambda_{it}(\mathbf{y},\boldsymbol{\omega})(d_{it}^{\mathrm{RT}}-\bar{D}_{it})^+. \tag{8}$$

Note that unlike $\mathcal{T}^{\mathrm{DA}}$, the time intervals in $\mathcal{T}^{\mathrm{RT}}$ could have a finer granularity than 1 hour, as in practice real-time models may be solved every 5 or 15 minutes. Let $\mathcal{T}^{\mathrm{RT|Hour}}$ be the set of hours in $\mathcal{T}^{\mathrm{RT}}$. Then $N^{\mathrm{tp}} = \frac{|\mathcal{T}^{\mathrm{RT}}|}{|\mathcal{T}^{\mathrm{RT|Hour}}|}$ is the number of time periods per hour. For example, if the real-time time interval is 5 minutes, then there are 12 time intervals per hour. We point out that (8) is nonconvex because of the bilinear term $\lambda_{it}(\mathbf{y},\boldsymbol{\omega})d_{it}^{\mathrm{RT}}$ and the expression $(d_{it}^{\mathrm{RT}}-\bar{D}_{it})^+$.

Note that several quantities in this expression are unknown at the time of the day-ahead computation, i.e., for a given $\mathbf{y}$; therefore, V is a random variable. Thus, a major component of our algorithm is the estimation of $\hat{V}$, the risk term in (1), as a *robust* estimate for V, through appropriate constraints to be added, incrementally, to the formulation of our risk-averse SCUC problem. Section II-B describes the robust modeling of V and algorithmic details are deferred to Section III.

(7) *Full Formulation:* We now present the risk-aware SCUC optimization problem in full.

$$\min \sum_{t\in\mathcal{T}^{\mathrm{DA}}}\Big(\sum_{g\in\mathcal{G}}\big(h_{gt}+C_g^{\mathrm{Start}}v_{gt}+C_g^{\mathrm{Down}}w_{gt}\big) + \sum_{i\in\mathcal{N}}C^{\mathrm{VOLL}}p_{it}^{\mathrm{Unmet}}\Big)+\rho\hat{V}(\mathbf{y}) \tag{9a}$$

$$\text{s.t. } (2),(3),(4),(6) \qquad \forall t\in\mathcal{T}^{\mathrm{DA}} \tag{9b}$$

$$(5) \tag{9c}$$

(7) $\forall t \in \mathcal{T}^{\mathrm{DA}} \setminus \{1\}$ (9d)

$$\hat{V}(\mathbf{y}) = \max_{\boldsymbol{\omega} \in \Omega} \frac{1}{N^{\mathrm{tp}}} \sum_{t \in \mathcal{T}^{\mathrm{RT}}} \sum_{i \in \mathcal{N}} \lambda_{it}(\mathbf{y}, \boldsymbol{\omega})(d_{it}^{\mathrm{RT}} - \bar{D}_{it})^{+} \tag{9e}$$

where Ω is an uncertainty set that includes *reasonable, but stress-revealing* real-time parameters – in Section II-C we will indicate how this set Ω is constructed in a data-driven manner. Constraints (9b) - (9d) include all constraints in a standard SCUC problem. Constraint (9e) provides a robust estimate for the consumer cost. Note that this constraint models the maximum of the consumer cost expression (8) over the uncertainty set. To handle this nonconvex constraint, we describe a decomposition algorithm that replaces (9e) with linear cutting planes in Section III-A.

B. Adversarial Real-time Operations

We now describe our methodology for attaining a measure of robustness in our estimate $\hat{V} = \hat{V}(\mathbf{y})$, which is the (uncertain) real-time consumer cost V given a UC decision $\mathbf{y}$. To that end, we next describe our formulation for the uncertain real-time direct-current optimal power flow (DCOPF) problem. We consider uncertainty in both real-time load d_{it}^{RT} and real-time wind generation $p_{gt}^{\max,\mathrm{RT}}$, and let $\mathbf{d}^{\mathrm{RT}}$ and $\mathbf{p}^{\max,\mathrm{RT}}$ be their corresponding vectors. We assume that the pair $(\mathbf{d}^{\mathrm{RT}}, \mathbf{p}^{\max,\mathrm{RT}})$ belongs to the uncertainty set Ω, and thus $\boldsymbol{\omega} = (\mathbf{d}^{\mathrm{RT}}, \mathbf{p}^{\max,\mathrm{RT}})$. Given a set of commitment decisions, we are interested in the pair $(\mathbf{d}^{\mathrm{RT}}, \mathbf{p}^{\max,\mathrm{RT}}) \in \boldsymbol{\Omega}$ that attains the peak consumer cost. To construct such a pair, we denote the vector of the DCOPF problem decision variables as $\mathbf{x}^{\mathrm{RT}}$, the vector of all fixed commitment decisions (selected day-ahead) as $\mathbf{y}^*$, the DCOPF feasible region as $X^{\mathrm{RT}}(\mathbf{y}^*, \boldsymbol{\omega})$, which is parameterized by commitment decisions and uncertain quantities, and the DCOPF problem itself as DCOPF$(\mathbf{y}^*, \boldsymbol{\omega})$, which is defined as follows:

$$\min_{\mathbf{x}^{\mathrm{RT}} \in X^{\mathrm{RT}}(\mathbf{y}^*, \boldsymbol{\omega})} \sum_{t \in \mathcal{T}^{\mathrm{RT}}} \left(\sum_{g \in \mathcal{G}} h_{gt} + \sum_{i \in \mathcal{N}} C^{\mathrm{VOLL|RT}} p_{it}^{\mathrm{Unmet}} \right). \tag{10}$$

Note that we set the real-time VOLL $C^{\mathrm{VOLL|RT}} > C^{\mathrm{VOLL}}$ to penalize unsatisfied real-time load.

Next, the right-hand side (RHS) of the load constraint (3a) is replaced with real-time load d_{it}^{RT}:

$$\sum_{g \in \mathcal{G}_i} p_{gt} + p_{it}^{\mathrm{Unmet}} + \sum_{(j,i) \in \mathcal{L}} f_{jit} - \sum_{(i,j) \in \mathcal{L}} f_{ijt} = d_{it}^{\mathrm{RT}} \quad \forall i \in \mathcal{N}. \tag{11}$$

The dual of this constraint is the real-time LMP λ_{it}.

In addition, we fix the commitment decisions in constraints (2), (6a) and (6b), and replace the RHS of (6c) with real-time wind generation:

$$h_{gt} \geq C_{og}^{1} p_{gt} + C_{og}^{0} y_{gt}^{*} \qquad \forall o \in \mathcal{O}, g \in \mathcal{G}^{\mathrm{Ther}} \tag{12a}$$

$$p_{gt} \leq P_{g}^{\max} y_{gt}^{*} \qquad \forall g \in \mathcal{G}^{\mathrm{Ther}} \tag{12b}$$

$$p_{gt} \geq P_{g}^{\min} y_{gt}^{*} \qquad \forall g \in \mathcal{G}^{\mathrm{Ther}} \tag{12c}$$

$$p_{gt} + p_{gt}^{\mathrm{Curtail}} = p_{gt}^{\max,\mathrm{RT}} \qquad \forall g \in \mathcal{G}^{\mathrm{Wind}}. \tag{12d}$$

To reformulate (7), note that in real time the ramping rate M_g is prorated to M_g^{RT} based on the time intervals in $\mathcal{T}^{\mathrm{RT}}$. Denoting the real-time limit on ramping as $\hat{M}_g$. Then $\hat{M}_g = M_g^{\mathrm{RT}}$ if $y_{g,t-1}^* = y_{g,t}^* = 1$, i.e., when the generator is on for both the previous and current time intervals; Otherwise, $\hat{M}_g = P_g^{\min}$. Constraints (7) are reformulated as:

$$p_{gt} - p_{g,t-1} \leq \hat{M}_g \qquad \forall g \in \mathcal{G}^{\mathrm{Ther}} \tag{13a}$$

$$p_{g,t-1} - p_{gt} \leq \hat{M}_g \qquad \forall g \in \mathcal{G}^{\mathrm{Ther}} \tag{13b}$$

Hence, the feasible region of the DCOPF problem, given the UC decision $\mathbf{y}^*$ and realization $\boldsymbol{\omega}$, is defined as follows:

$$X^{\mathrm{RT}}(\mathbf{y}^*, \boldsymbol{\omega}) := \left\{ \mathbf{x}^{\mathrm{RT}} \;\middle|\; \begin{matrix} (3b), (4), (6d), (6e) \\ (11), (12), (13) \end{matrix} \;, \forall t \in \mathcal{T}^{\mathrm{RT}} \right\}.$$

Above, to simplify notation, we re-use notation for day-ahead decision variables (e.g. h_{gt} and p_{gt}) in the real-time problem, in which case they represent real-time decisions. In what follows, the dual of the DCOPF problem given $\mathbf{y}^*$ and $\boldsymbol{\omega}$ will be denoted by DCOPF-D$(\mathbf{y}^*, \boldsymbol{\omega})$.

We now describe how to implement constraint (9e). First, the real-time LMP λ_{it} (again given $\mathbf{y}^*$ and $\boldsymbol{\omega}$) is an optimal solution to DCOPF-D$(\mathbf{y}^*, \boldsymbol{\omega})$. Thus, (9e) amounts to finding uncertain quantities and resulting real-time LMPs that maximize the consumer cost in the critical time period $\mathcal{T}^{\mathrm{RT}}$, as given in (8). We define the adversarial DCOPF problem as:

DCOPF-A$(\mathbf{y}^*) :=$

$$\max_{\boldsymbol{\omega} \in \Omega} \frac{1}{N^{\mathrm{tp}}} \sum_{t \in \mathcal{T}^{\mathrm{RT}}} \sum_{i \in \mathcal{N}} \lambda_{it}(\mathbf{y}^*, \boldsymbol{\omega})(d_{it}^{\mathrm{RT}} - \bar{D}_{it})^{+} \tag{14a}$$

$$\text{s.t.} \quad \lambda_{it}(\mathbf{y}^*, \boldsymbol{\omega}) \text{ is an optimal solution of DCOPF-D}(\mathbf{y}^*, \boldsymbol{\omega}). \tag{14b}$$

One way to write constraint (14b) explicitly, is to write a primal-dual formulation for DCOPF$(\mathbf{y}^*, \boldsymbol{\omega})$ and utilize strong duality, as in [33]. However, since (14a) and the resulting strong duality constraint are nonlinear, DCOPF-A$(\mathbf{y}^*)$ may be difficult to solve. As an alternative, in Section III-C we present a grid search method to approximately solve DCOPF-A$(\mathbf{y}^*)$ and find adversarial stressors.

C. Data-Driven Uncertainty Set

Our choice of the uncertainty set Ω is driven by the goal to adapt the SCUC computation to better deal with *volatility*. Toward this end, our uncertainty set Ω is constructed through an approximate, PCA (principal component analysis)-driven representation of the *covariance* of loads and renewable outputs. Both load and renewable exhibit locational correlation and we find that a few leading modes of the covariance matrix are sufficient to explain total variability [34]. The particular methodology we follow is motivated by the "factor stressing" technique employed in the financial services industry [22].

More specifically, for each time $t \in \mathcal{T}^{\mathrm{RT}}$ we obtain data for *recent past* (e.g. hourly observations in the past month), and use such data to construct a covariance matrix. The number of rows of the load covariance matrix equals $|\mathcal{N}|$ and the number of rows of the wind covariance matrix equals the number of wind farms. We conduct a spectral decomposition on a covariance matrix to obtain its eigenvalues and standardized eigenvectors. The eigenvectors corresponding to the K largest eigenvalues (sorted from large to small), i.e., the K leading modes, are used to construct our set Ω.

Let us consider loads (a similar process is used for wind). Let $k \in \{1, \ldots, K\}$ be the index for the leading modes, and

$\mathbf{Q}^d_{kt} := (Q^d_{k1t}, Q^d_{k2t}, \ldots, Q^d_{k|\mathcal{N}|t})^\top$ be the vector of the kth eigenvector for load at time t. We will construct a quantity $\alpha^d_{kt} \geq 0$, which is the "stressor" that magnifies the load variability along the kth leading mode at time t. Similarly, $\mathbf{Q}^w_{kt}$ and α^w_{kt} are eigenvector and stressor of wind power.

Using this notation we can describe the formal set Ω from which we select our load d^{RT}_{it} and wind power $p^{\max,\mathrm{RT}}_{gt}$ scenarios. It is given by the pairs $(d^{\mathrm{RT}}_{it}, p^{\max,\mathrm{RT}}_{gt})$ satisfying:

$$d^{\mathrm{RT}}_{it} = \bar{D}_{it} + \sum_{k=1}^{K} Q^d_{kit}\alpha^d_{kt} \qquad \forall i \in \mathcal{N}, t \in \mathcal{T}^{\mathrm{RT}} \quad (15a)$$

$$p^{\max,\mathrm{RT}}_{gt} = \bar{P}^{\max}_{gt} + \sum_{k=1}^{K} Q^w_{kgt}\alpha^w_{kt} \qquad \forall g \in \mathcal{G}^{\mathrm{Wind}}, t \in \mathcal{T}^{\mathrm{RT}} \quad (15b)$$

$$|\sum_{k=1}^{K} \alpha^{ind}_{kt}| \leq \Sigma^{ind} \qquad \forall t \in \mathcal{T}^{\mathrm{RT}}, ind \in \{d, w\} \quad (15c)$$

$$|\alpha^{ind}_{kt}| \leq R^{ind} \ \forall k = 1, \ldots, K; t \in \mathcal{T}^{\mathrm{RT}}, ind \in \{d, w\} \quad (15d)$$

$$d^{\mathrm{RT}}_{it} \geq 0 \qquad \forall i \in \mathcal{N}, t \in \mathcal{T}^{\mathrm{RT}} \quad (15e)$$

$$p^{\max,\mathrm{RT}}_{gt} \geq 0 \qquad \forall g \in \mathcal{G}^{\mathrm{Wind}}, t \in \mathcal{T}^{\mathrm{RT}}. \quad (15f)$$

Constraints (15a) represent the real-time load scenarios as the sum of the forecast and stressed leading modes. Similar expressions are derived for wind power in constraints (15b). Constraints (15c) and (15d) bound the stressors and control the level of conservatism. Constraints (15e) and (15f) ensure load and wind power are non-negative.

III. Solution Approach

Solving the risk-aware optimization model (9) directly (e.g., using off-the-shelf solvers) is difficult because the first-stage problem contains both integer variables and bilinear terms (in constraint (9e)). In Section III-A, we show how to solve this two-stage problem (9) by relying on an iterative decomposition algorithm that approximates constraint (9e) with increasing accuracy. The procedure is guaranteed to finitely terminate with an optimal solution to (9). Section III-B introduces the cutting planes used in the procedure. Section III-C describes an adversarial procedure that is used to improve the accuracy of the approximate formulation. We include additional implementation details in Section III-D.

A. Decomposition Algorithm

To solve (9), we rely on an iterative method which is similar to the Benders' decomposition scheme [26]. We will next provide a simplified version of this method, and later we will amend this outline in order to handle integer variables.

Under this simplified procedure, at any intermediate point of the algorithm we will have a relaxation for (9) that we term the "master problem" which is initially obtained from (9) by removing (9e) and replacing it with $\hat{V} \geq 0$. As the procedure iterates, cuts are added to the master problem to approximate (9e) with increasing accuracy.

Suppose that at some iteration the solution to the master problem is given by vector $\mathbf{y}^*$. This vector may not solve problem (9) since it may not satisfy (9e). To check whether this is the case, $\mathbf{y}^*$ is input to a procedure given in Section III-C. If this procedure verifies that $\mathbf{y}^*$ is feasible for (9e), then $\mathbf{y}^*$ is optimal for (9). Otherwise, a cutting plane is generated for strengthening the master problem relaxation. Figure 2 provides an illustration of the procedure, which is a decomposition algorithm. In this figure, $\mathcal{P}^{\mathrm{Master}}$ is the master problem and DCOPF-A($\mathbf{y}^*$) is the adversarial problem given $\mathbf{y}^*$. Additional algorithmic details such as grid search, partially fixing $\mathbf{y}$, and branch-and-cut will be introduced in later sections.

More specifically, the initial master problem $\mathcal{P}^{\mathrm{Master}}$ is:

$$\begin{aligned} \mathcal{P}^{\mathrm{Master}} := \min \quad & (1) \\ \text{s.t.} \quad & (2), (3), (4), (6) \qquad \forall t \in \mathcal{T}^{\mathrm{DA}} \\ & (5), \hat{V} \geq 0 \\ & (7) \qquad \forall t \in \mathcal{T}^{\mathrm{DA}} \setminus \{1\}. \end{aligned}$$

This master problem includes the integer unit-commitment variables, which necessitates an appropriate adjustment to the proposed methodology, as explained in Section III-D.

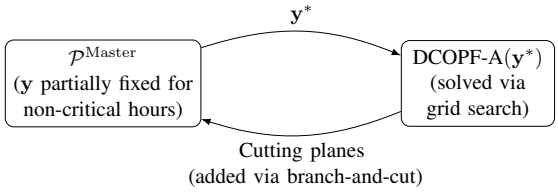

Fig. 2: The decomposition algorithm

B. Cutting Planes

The cutting planes we use include no-good [35], integer L-shaped [28], and LBBD cuts [29]. Together these cuts yield a lower bound for the worst-case consumer cost V given UC decision $\mathbf{y}$. These cuts have the generic form $\hat{V}(\mathbf{y}) \geq f(\mathbf{y})$, where $f(\mathbf{y})$ is a linear function of the commitment decisions $\mathbf{y}$, and satisfies the following conditions:

- For all feasible UC decisions of $\mathbf{y}$, $f(\mathbf{y})$ must be an underestimator for the worst-case consumer cost given $\mathbf{y}$, i.e., $\max_{\boldsymbol{\omega}\in\Omega} \frac{1}{N^{\mathrm{tp}}} \sum_{t\in\mathcal{T}^{\mathrm{RT}}} \sum_{i\in\mathcal{N}} \lambda_{it}(\mathbf{y}, \boldsymbol{\omega})(d^{\mathrm{RT}}_{it} - \bar{D}_{it})^+$. Moreover, the inequality $\hat{V}(\mathbf{y}) \geq f(\mathbf{y})$ should cut off the current master problem solution.
- Let $\mathbf{y}^*$ be the commitment decisions in the current master problem solution. In a neighborhood of $\mathbf{y}^*$, $f(\mathbf{y})$ should, in addition, be a close lower bound to the worst-case consumer cost given $\mathbf{y}$. The strength of the cut rests on how close this approximation is.

We first present a no-good cut which only provides a good lower bound at the current solution $\mathbf{y}^*$, then we develop integer L-shaped cuts and LBBD cuts that aim to improve this lower bound for solutions in a neighborhood of $\mathbf{y}^*$. Throughout, we assume that the worst-case consumer cost given $\mathbf{y}^*$ is attained by profile ω^* (including loads $d^{\mathrm{RT}*}_{it}$), i.e., that $\hat{V}^* = \hat{V}^*(\mathbf{y}^*) := \frac{1}{N^{\mathrm{tp}}} \sum_{i\in\mathcal{N}} \sum_{t\in\mathcal{T}^{\mathrm{RT}}} \lambda_{it}(\mathbf{y}^*, \boldsymbol{\omega}^*)(d^{\mathrm{RT}*}_{it} - \bar{D}_{it})^+$.

1) No-good Cuts

Let $\mathbf{y}^*$ be the commitment decisions in the current master problem solution. Define $\mathcal{I}_{1t} = \{ g \mid y^*_{gt} = 1, \forall g \in \mathcal{G}^{\mathrm{Ther}} \}$ and $\mathcal{I}_{0t} = \{ g \mid y^*_{gt} = 0, \forall g \in \mathcal{G}^{\mathrm{Ther}} \}$ respectively as the set of thermal generators that are on/off at time t. Let $d^{\mathrm{RT}*}_{it}$ and λ^*_{it} be the optimal primal and dual solution values, in

DCOPF-A($\mathbf{y}^*$), for d_{it}^{RT} and λ_{it}, respectively. The no-good cut is as follows:

$$\hat{V}(\mathbf{y}) \geq \hat{V}^*(\mathbf{y}^*)\left(1 - \sum_{t\in\mathcal{T}^{\mathrm{RT|Hour}}}\left(\sum_{g\in\mathcal{I}_{1t}}(1-y_{gt}) + \sum_{g\in\mathcal{I}_{0t}} y_{gt}\right)\right). \tag{16}$$

When $y_{gt} = y^*_{gt}, \forall g \in \mathcal{G}^{\mathrm{Ther}}, t \in \mathcal{T}^{\mathrm{RT|Hour}}$, the cut can be simplified to $\hat{V}(\mathbf{y}) \geq \hat{V}^*(\mathbf{y}^*)$, which provides the correct value for $\hat{V}(\mathbf{y})$. Otherwise, when at least one generator in $\mathcal{I}_{1t}$ is turned off or at least one generator in $\mathcal{I}_{0t}$ is turned on during $\mathcal{T}^{\mathrm{RT}}$, the RHS of the cut becomes non-positive.

The no-good cut is not very strong as it only provides a good underestimator at the current master solution. In fact, as there are $2^{|\mathcal{G}^{\mathrm{Ther}}||\mathcal{T}^{\mathrm{RT|Hour}}|}$ possible values for the vector $\mathbf{y}$, the algorithm could run through $\mathcal{O}(2^{|\mathcal{G}^{\mathrm{Ther}}||\mathcal{T}^{\mathrm{RT|Hour}}|})$ iterations to find the optimal solution if only no-good cuts are used.

2) Integer L-Shaped Cuts

The integer L-shaped cut strengthens the no-good cut by improving a lower bound at some feasible commitment solutions in a neighborhood of $\mathbf{y}^*$:

$$\hat{V}(\mathbf{y}) \geq \hat{V}^*(\mathbf{y}^*) + a\sum_{t\in\mathcal{T}^{\mathrm{RT|Hour}}}\left(\sum_{g\in\mathcal{I}_{1t}} y_{gt} - \sum_{g\in\mathcal{I}_{0t}} y_{gt} - |\mathcal{I}_{1t}|\right), \tag{17}$$

where $a = \max(\hat{V}^* - \hat{V}_1, (\hat{V}^* - \hat{V}_0)/2)$, $\hat{V}_1$ equals the minimum value of the consumer cost when exactly one generator changes its commitment decision (i.e., when $\sum_{g\in\mathcal{I}_{1t}} y_{gt} - \sum_{g\in\mathcal{I}_{0t}} y_{gt} = |\mathcal{I}_{1t}|-1$, which we call the *1-neighbors* of $\mathbf{y}^*$), and $\hat{V}_0$ is a lower bound on the consumer cost under a feasible commitment decision (e.g., trivially $\hat{V}_0 = 0$ can be used).

To see that the cut is valid, notice that for the 1-neighbors of $\mathbf{y}^*$, the integer L-shaped cut provides a lower bound for $\hat{V}(\mathbf{y})$, namely $\hat{V}(\mathbf{y}) \geq \min(\hat{V}_1, \frac{\hat{V}^*+\hat{V}_0}{2})$. This lower bound is valid because $\min(\hat{V}_1, \frac{\hat{V}^*+\hat{V}_0}{2}) \leq \hat{V}_1$. And if there is more than one generator that changes its commitment decision, then the RHS of (17) is no more than $\hat{V}_0$, and thus is valid.

Note that to obtain $\hat{V}_1$, we could solve DCOPF-A($\mathbf{y}^*$) for each $\mathbf{y}$ among the 1-neighbors of $\mathbf{y}^*$, which requires solving $|\mathcal{T}^{\mathrm{RT|Hour}}|(|\mathcal{G}^{\mathrm{Ther}}|-1)$ subproblems. In our experiments, we observe that the integer L-shaped cuts indeed lead to faster convergence than the no-good cuts. We point out that since $\min(\hat{V}_1, \frac{\hat{V}^*+\hat{V}_0}{2}) \geq 0$, it is generally a better lower bound than that provided by a no-good cut. However, the computational efforts to generate an L-shaped cut increases as more subproblems are solved to get $\hat{V}_1$.

3) LBBD Cuts

Another way to strengthen the no-good cut is to use the following LBBD cut:

$$\hat{V}(\mathbf{y}) \geq \sum_{t\in\mathcal{T}^{\mathrm{RT|Hour}}}\left(\hat{V}_t^*(\mathbf{y}^*)\left(1 - \sum_{g\in\mathcal{I}_{0t}} y_{gt}\right)\right), \tag{18}$$

where $\hat{V}_t^*(\mathbf{y}^*) := \frac{1}{N^{\mathrm{tp}}}\sum_{\tau\in\mathcal{T}^{\mathrm{RT}}(t)}\sum_{i\in\mathcal{N}}\lambda_{i\tau}(\mathbf{y}^*, \boldsymbol{\omega}^*)(d_{i\tau}^{\mathrm{RT}*} - \bar{D}_{i\tau})^+$, with $\mathcal{T}^{\mathrm{RT}}(t)$ being the set of real-time time periods in hour t. Note that $\hat{V}^*(\mathbf{y}^*) = \sum_{t\in\mathcal{T}^{\mathrm{RT|Hour}}}\hat{V}_t^*(\mathbf{y}^*)$. When any generator in $\mathcal{I}_{0t}$ is turned on, the term corresponding to hour t in the RHS becomes non-positive. On the other hand, if all generators in $\mathcal{I}_{0t}$ stay off, then this cut enforces that the consumer cost is at least $\hat{V}_t^*(\mathbf{y}^*)$. Intuitively, if all generators in $\mathcal{I}_{0t}$ and some generators in $\mathcal{I}_{1t}$ are turned off, the consumer cost is not likely to drop. In Proposition III.1, we prove that this lower bound is valid when the network is not congested and the ramping constraints are not binding in the real-time market. As we will also explain, the cut is still good for our purpose even when those restrictions are relaxed.

Proposition III.1. *When there is no congestion in the network and the ramping constraints are not binding in the real-time market, the LBBD cut* (18) *provides a correct lower bound for* $\hat{V}(\mathbf{y})$. *Also, it provides the exact value of* $\hat{V}(\mathbf{y})$ *at the current solution* $\mathbf{y}^*$.

Proof. Since there is no congestion, the LMPs at all nodes are equal, which we denote as λ_t.

Consider the fixed wind and load profile $\boldsymbol{\omega}^*$ that defines the worst-case for $\mathbf{y}^*$ and fixed hour $t \in \mathcal{T}^{\mathrm{RT|Hour}}$. Let $\mathbf{y}'$ be a feasible dispatch solution from the master problem, and $\mathcal{I}'_{1t}$ and $\mathcal{I}'_{0t}$ respectively be the corresponding set of generators that are on and off at t. We will show that the consumer cost term arising from hour t, namely $\hat{V}_t^*(\mathbf{y}^*)\left(1 - \sum_{g\in\mathcal{I}_{0t}} y_{gt}\right)$, is a lower bound for the consumer cost at t, if we switch from $\mathbf{y}^*$ to $\mathbf{y}'$. We consider the following two cases:

Case 1: If $\mathcal{I}'_{0t} \subset \mathcal{I}_{0t}$ for some $t \in \mathcal{T}^{\mathrm{RT|Hour}}$, then $\sum_{g\in\mathcal{I}_{0t}} y'_{gt} \geq 1$, which indicates that the RHS of (18) corresponding to t is no more than 0.

Case 2: If all generators that were off during t under $\mathbf{y}^*$ remain off under $\mathbf{y}'$, then $\mathcal{I}_{0t} \subseteq \mathcal{I}'_{0t}$ and the RHS of (18) corresponding to t remains unchanged. Thus, we need to show that this RHS value is a valid lower bound.

This is the same as showing that the LMP at every time $\tau \in \mathcal{T}^{\mathrm{RT}}(t)$ does *not* decrease when we switch from $\mathbf{y}^*$ to $\mathbf{y}'$. To see this, note that any generator g that is on at time τ under $\mathbf{y}^*$ must be of one of three types:

(a) It defines the LMP, i.e., $h_{g,\tau} = \lambda_\tau$, or

(b) It satisfies $h_{g,\tau} < \lambda_\tau$, in which case the generator is operating at its maximum output, or

(c) The generator satisfies $h_{g,\tau} > \lambda_\tau$, in which case the generator is operating at its *minimum* output level.

Moreover, the total load is equal to the maximum output of the generators in type (b), plus the minimum output from generators of type (c), plus the output of the generators of type (a). A similar characterization can be obtained for $\mathbf{y}'$. From this characterization it is clear that if we turn off a generator the LMP cannot decrease, since turning a generator off reduces total available capacity, and thus the new LMP will be defined either by a generator of type (a) under $\mathbf{y}^*$ (in which case the LMP does not change) or by a generator of type (c) under $\mathbf{y}^*$, in which case the LMP strictly increases. The new LMP could also equal C^{VOLL}, which is the highest value it can reach.

Finally, if $\mathbf{y}' = \mathbf{y}^*$, then the RHS of (18) provides the exact value for the worst-case consumer cost. □

Note that when there is congestion in the network, the result in Case 2 of the proof may not hold because prices could drop at certain locations even if only a strict subset of generators are turned on. Also, if some of the ramping constraints are binding, then the production variables at $t-1$ and t are coupled, which complicates the proof of Case 2, as the selection of marginal generator could be affected by the production levels of previous time periods (an example for this is provided in Appendix A).

Although we are not able to provide a formal proof for the quality of the cut in the general case, in our experiments we observe that using LBBD cuts with the decomposition algorithm returns correct solutions for the majority of instances. Note that the NYISO system in our case study does not have a lot of congestion. Also, $\mathcal{T}^{\mathrm{RT}}$ in Section IV-B of the case study contains a single time period and thus the real-time problem does not have ramping constraints. Even if the cut leads to an overestimation (which is usually very small) of the consumer cost, it may only lead to less adversarial stressors, which may still provide robust enough SCUC solutions.

The LBBD cut implies the no-good cut (16), and thus is strictly stronger than the no-good cut. Also, the LBBD cuts lead to much faster convergence compared with no-good cuts and do not require extra computational efforts to generate like for the integer L-shaped cuts.

C. Solving DCOPF-A($\mathbf{y}^*$)

Instead of directly solving the nonconvex problem DCOPF-A($\mathbf{y}^*$), we employ grid search to solve it approximately. In grid search, we iterate through a set of fixed stressors (i.e, "grids") $(\tilde{\alpha}^d_{kt}, \tilde{\alpha}^w_{kt})$ that satisfy constraints (15), and find the stressors that lead to the highest consumer cost.

More specifically, for each fixed pair of stressors $(\tilde{\alpha}^d_{kt}, \tilde{\alpha}^w_{kt})$, we obtain the corresponding scenario $\tilde{\boldsymbol{\omega}}$ using (15a) and (15b), and solve DCOPF($\mathbf{y}^*, \tilde{\boldsymbol{\omega}}$). We then calculate the corresponding consumer cost. Among all consumer costs calculated in this way, we select the highest one as an estimate to the optimal value of DCOPF-A($\mathbf{y}^*$), and the corresponding DCOPF($\mathbf{y}^*, \tilde{\boldsymbol{\omega}}$) problem provides the optimal solutions for adverse load and wind generation scenarios, and the LMPs.

The grid search method provides an approximation to the true objective of DCOPF-A($\mathbf{y}^*$). It is difficult to directly solve the highly nonlinear and nonconvex DCOPF-A($\mathbf{y}^*$) problem, even with state-of-the-art nonlinear optimization solvers such as Gurobi and Knitro. We also observe that the commonly-used McCormick relaxation is not very tight for nonlinear terms in DCOPF-A($\mathbf{y}^*$). On the other hand, with a carefully-selected set of grids in the grid search, we can find adverse scenarios that lead to cost-saving UC decisions. We explain how to select the set of grids in Section IV-A.

D. Implementation Details

The decomposition algorithm in Section III-A requires solving a MIP master problem in each iteration, which is time consuming. Therefore, we instead add the cuts via branch-and-cut [27], where we solve the master problem once and the violated cuts are added in the integral nodes of the branch-and-bound tree. We observe that branch-and-cut greatly improves the performance of our algorithm.

Among the three types of cuts derived in Section III-B, we can use any one of them or a combination of them in our algorithm. Note that integer L-shaped cuts and LBBD cuts are both stronger than no-good cuts, so there is no need to use no-good cuts if either of the two other cuts is used. Between integer L-shaped cuts and LBBD cuts, one does not dominate the other in terms of strength, so it could be helpful to include both cuts in the algorithm. Since it is time consuming to generate integer L-shaped cuts for large-scale problems, we use only LBBD cuts in our case study.

Compared with commitment decisions from the deterministic SCUC problem, the risk-aware solution usually keeps more capacities committed around critical hours that are represented by the real-time market problem. Therefore, we can speed up the algorithm by only allowing commitment decisions around critical hours to deviate from its deterministic counterpart, which greatly reduces the search space of binary on/off decisions.

IV. NYISO Case Study

A. Data Resource and Simulation Environment

For the numerical experiments we use an NYISO dataset including 1819 buses, 2207 lines, 362 generators and 38 wind farms [34]. Note that the 38 wind farms include 33 onshore wind farms that are already built, and 5 offshore farms under construction. The wind power data are calculated from the expected and real-time wind speed in August 2013, obtained from the NREL WIND Toolkit [36]. The load data are from the NYISO data platform [37]. Due to data availability, we use the load data from August 2018. We use real-time wind power and load data of the whole month to calculate leading modes, and pick a windy day in the month to solve the SCUC problem. We choose the number of leading modes $K = 3$ because from empirical experience the first three components are enough to explain most variability (more precisely, the three leading eigenvalues account of almost all of the Frobenius norm of the appropriate covariance matrix). The day-ahead and real-time VOLL are respectively set at 10,000 \$/MWh and 20,000 \$/MWh. The set $\mathcal{T}^{\mathrm{RT}}$ includes the hour 6-7 pm, which is a time period with peak load, and we allow commitment decisions to deviate from its deterministic counterpart between 5 pm and 8 pm.

We generate the grids in grid search as follows. First, we fix $\Sigma^{ind} = 3R^{ind}$ and relax constraint (15c). We then allow the stressors α^{ind}_{kt} to be either R^{ind} or $-R^{ind}$ so for each time period t, there are a total of 8 (i.e., 2^3) possible grids. For wind generation $p^{\max,\mathrm{RT}}_{gt}$, we include all 8 grids, while for load d^{RT}_{it}, we include 2 grids, $[R^d, -R^d, R^d]$ and $[R^d, R^d, -R^d]$, which are usually the most adverse stressors. Note that when R^{ind} is large, it is possible that d^{RT}_{it} or $p^{\max,\mathrm{RT}}_{gt}$ becomes negative at one of the grids. If this happens, we adjust the value of the third stressor α^{ind}_{3t} to the largest (if $\alpha^{ind}_{3t} = R^{ind}$) or the smallest (if $\alpha^{ind}_{3t} = -R^{ind}$) value that ensures nonnegativity of $d^{\mathrm{RT}}_{it}/p^{\max,\mathrm{RT}}_{gt}$.

We run all experiments on a Linux workstation with Intel Xeon processor and 250 GB memory. The programming language is Python v3.8. Optimization problems are solved

with Gurobi 10.0.1. For the master problem, we set the MIP gap to 10^{-3}, and the time limit to 24 hours. All instances are solved to within 0.5% optimality gap upon termination.

B. Performance of Risk-Aware Model

Table I shows the comparison between results from risk-aware and deterministic SCUC problems with different bounds for stressors. R^d takes the values 0.1 and 0.2, and R^w varies from 0.2 to 1.0 with stepsize 0.2. The weight for consumer cost $\rho = 1$. The column "Save" shows the saving of the risk-aware SCUC compared with the deterministic SCUC in total costs; "Deter. cost" reports the total costs of the deterministic SCUC; "Cost red." equals "Save" divided by "Deter. cost"; "DA cost diff" is the extra day-ahead cost for carrying out the risk-aware dispatch decisions; "Consr. cost" is the consumer cost in risk-aware SCUC. In addition, Table II lists the change in total load and wind generation under the selected adverse scenarios. The change in load is calculated as (Total load under adverse scenario - Total expected load)/(Total expected load). The change in wind generation is compared with total expected load, and is calculated as (Total wind generation under adverse scenario - Total expected wind generation)/(Total expected load). Note that for some instances (distinguished by $*$ in the tables) we add 3 cuts at the root node of the branch-and-cut algorithm to bring the optimality gap below 0.5%.

TABLE I: Comparison of Risk-Aware and Deterministic SCUC Problems for $\rho = 1$

R^d	R^w	Save (k$)	Deter. cost (M$)	Cost red. (%)	DA cost diff ($)	Consr. cost (k$)
0.1	0.2	0.00	5.37	0.00	0.00	8.53
0.1	0.4	0.12	5.37	0.00	116.16	8.53
0.1	0.6	0.00	5.37	0.00	0.00	8.89
0.1	0.8	42.29	5.41	0.78	116.16	8.89
0.1	1.0	42.28	5.41	0.78	123.50	8.89
0.2	0.2	114.71	5.50	2.09	116.16	17.78
*0.2	0.4	114.14	5.50	2.08	688.03	17.78
0.2	0.6	115.74	5.50	2.11	1446.22	16.76
0.2	0.8	108.58	5.50	1.98	8130.20	17.78
*0.2	1.0	115.64	5.50	2.10	1072.06	17.78

* Instance solved with 3 root cuts.

TABLE II: Change in Load and Wind Generation (Compared with Total Expected Load) Under Adverse Scenario for $\rho = 1$

R^d	R^w	Load (%)	Wind (%)
0.1	0.2	1.18	-0.37
0.1	0.4	1.18	-0.74
0.1	0.6	1.18	-1.11
0.1	0.8	1.18	-1.44
0.1	1.0	1.18	-1.97
0.2	0.2	2.36	-0.37
*0.2	0.4	2.36	-0.74
0.2	0.6	2.36	-1.41
0.2	0.8	2.36	-1.75
*0.2	1.0	2.36	-1.97

* Instance solved with 3 root cuts.

The risk-aware SCUC reduces total costs for instances with higher variations. When the variation in load and wind generation increases, there tend to be more savings. The change in R^d has a larger impact on cost saving and consumer cost compared with the change in R^w. This is probably because compared with the impact of R^w, an increase in R^d leads to a higher change in load, as shown in Table II. Also, note that the cost saving does not necessarily increase monotonically with R^w, as the total costs of both SCUC models increase with more volatility.

The risk-aware SCUC has a slightly higher day-ahead cost due to the dispatch of additional generation capacity. This is a relatively small addition compared with the cost saving by implementing the risk-aware commitment decisions.

There is a threshold for volatility above which the risk-aware SCUC may no longer induce cost savings, as it becomes cheaper to pay the consumer cost than dispatching additional capacity. Such threshold tends to be lower with lower values of C^{VOLL} and ρ, which signals a less conservative risk-aware model.

To demonstrate how ρ affects conservatism, Table III shows the comparison of the two SCUC problems when $\rho = 0.1$. The risk-aware SCUC provides very similar dispatch decisions as the deterministic SCUC when the variations are low or very high. This is because at those volatility levels it is more expensive to mitigate the risk by altering the commitment decisions, and it is not economic to do so given the low weight assigned to consumer cost.

TABLE III: Comparison of Risk-Aware and Deterministic SCUC Problems for $\rho = 0.1$

Rd	Rw	Save (k$)	Deter. cost (M$)	Cost red. (%)	Op. cost diff ($)	Consr. cost (k$)
0.1	0.2	0.00	5.37	0.00	0.00	8.53
0.1	0.4	0.00	5.37	0.00	0.00	8.77
0.1	0.6	0.00	5.37	0.00	0.00	8.89
0.1	0.8	0.00	5.41	0.00	0.00	51.30
0.1	1	0.00	5.41	0.00	0.00	51.30
0.2	0.2	114.66	5.50	2.09	161.75	17.78
0.2	0.4	114.22	5.50	2.08	608.60	17.78
0.2	0.6	110.11	5.50	2.00	6050.39	17.78
0.2	0.8	0.00	5.50	0.00	0.00	134.50
0.2	1	0.00	5.50	0.00	0.00	134.50

Finally, note that the risk-aware model becomes more difficult to solve with an increase in the values of R^d, R^w, and ρ. Therefore, to achieve a model that balances computational efficiency and effectiveness, a practitioner needs to make thoughtful parameter selections.

C. Out-of-Sample Tests

In the previous section, we have shown that the risk-aware model leads to savings under an adverse realization picked by DCOPF-A($\mathbf{y}^*$). In this section, we test the robustness of the results under different realizations. In other words, we carry out "out-of-sample" tests to evaluate the dispatch decisions, by first obtaining dispatch decisions from risk-aware and deterministic SCUC models, and then formulating corresponding real-time DCOPF problems with simulated random realizations. This process allows us to assess the cost-saving and volatility reduction benefits of the risk-aware model.

More specifically, we randomly sample 100 realizations with two different methods, and evaluate the risk-aware model with both types of random samples. Note that for experiments in this section, the real-time DCOPF problem considers 5-minute time intervals in $\mathcal{T}^{\mathrm{RT}}$, providing a more realistic setup that mirrors real-life operations. As we will demonstrate shortly, even though the risk-aware dispatch solution is obtained based on 1-hour time interval, it still yields benefits

when the real-time problem is solved more frequently with smaller time intervals.

Our first experiment checks whether it is beneficial to use the risk-aware dispatch decisions under different adverse realizations. In particular, we perturb the selected adverse stressors $(\forall t \in \mathcal{T}^{\mathrm{RT}}, ind \in \{d, w\})$ $\boldsymbol{\alpha}^{ind*} = (\alpha_{1t}^{ind*}, \alpha_{2t}^{ind*}, \alpha_{3t}^{ind*})$ by randomly sample vectors with a fixed norm, where those vectors are uniformly distributed in a spherical cone centered at $\boldsymbol{\alpha}^{ind*}$ with the cone angle equals $\pi/3$. This perturbation fixes the magnitude of the adverse realization, while allowing the weight distribution to vary among the 3 leading modes to a certain degree. Using those random samples, we evaluate the risk-aware solutions under two different levels of conservatism with $R^d = 0.2, R^w = 0.2$ and $R^d = 0.2, R^w = 1.0$. The results are presented respectively in Table IV and Table V.

For both tables, we show the comparison between risk-aware and deterministic results when there are different bounds on stressors. R^d takes the values 0.1 and 0.2, and R^w takes values between 0.2 and 1.4 with stepsize 0.4. Columns "Save", "Cost red.", and "Consr. cost" have similar definitions as in Section IV-B, except that they are averaged over 100 random samples for out-of-sample evaluation. "Deter. std" and "RA. std" are respectively the average standard deviations of total cost under deterministic and risk-aware dispatch solutions.

TABLE IV: COMPARISON OF TWO SCUC SOLUTIONS OBTAINED FOR $R^d = 0.2, R^w = 0.2$, EVALUATED WITH PERTURBED ADVERSE REALIZATIONS

R^d	R^w	Save (k$)	Cost red. (%)	Consr. cost (k$)	Deter. std (k$)	RA. std (k$)
0.1	0.2	-0.04	0.00	7.55	0.46	0.43
0.1	0.6	2.31	0.04	8.33	3.49	1.91
0.1	1.0	4.07	0.08	11.16	4.13	3.25
0.1	1.4	2.97	0.06	16.06	4.30	4.11
0.2	0.2	17.57	0.32	49.71	20.34	16.29
0.2	0.6	15.40	0.28	49.51	15.71	13.34
0.2	1.0	11.86	0.22	54.63	13.62	13.68
0.2	1.4	7.86	0.14	57.28	13.60	13.53

TABLE V: COMPARISON OF TWO SCUC SOLUTIONS OBTAINED FOR $R^d = 0.2, R^w = 1.0$, EVALUATED WITH PERTURBED ADVERSE REALIZATIONS

R^d	R^w	Save (k$)	Cost red. (%)	Consr. cost (k$)	Deter. std (k$)	RA. std (k$)
0.1	0.2	-0.88	-0.02	7.43	0.45	0.43
0.1	0.6	0.70	0.01	7.44	2.59	0.44
0.1	1.0	4.47	0.08	7.42	3.63	0.43
0.1	1.4	9.76	0.18	8.26	4.48	1.72
0.2	0.2	51.33	0.94	15.27	19.48	0.99
0.2	0.6	43.48	0.80	17.87	15.46	4.72
0.2	1.0	37.17	0.68	24.81	13.51	8.43
0.2	1.4	31.31	0.58	31.73	13.85	10.43

In both Table IV and Table V, the risk-aware decisions save costs in almost all instances, despite the perturbation on realizations. Generally, the cost saving is larger under higher variations. Yet when there are extremely high variations the cost saving starts to decrease, as the extra capacity dispatched under the risk-aware solutions is not enough to keep LMPs below C^{VOLL} at many buses. We also note that the risk-aware dispatch decisions lead to lower volatility in total cost, as shown by the comparison of the standard deviations.

Compared with Table IV, Table V shows risk-aware solutions lead to higher savings and lower standard deviation in costs at high variation levels. Thus, to achieve more savings, it is important to adjust the values of R^d and R^w accordingly when formulating the risk-aware SCUC problem. For example, if for a certain day the real-time wind generation is expected to be very volatile, the practitioner should solve the risk-aware SCUC problem with a higher R^w value.

Our second experiment evaluates the benefit of risk-aware dispatch decisions under less adverse realizations. We generate samples of $\alpha_{kt}^{ind}(\forall k = 1, 2, 3; t \in \mathcal{T}^{\mathrm{RT}}, ind \in \{d, w\})$ that follow a uniform distribution in $[-R^{ind}, R^{ind}]$, and calculate corresponding realizations. Note that we truncate the realizations with a 0 lower bound to avoid negative load and wind generation. Again, we evaluate the dispatch solutions obtained with $R^d = 0.2, R^w = 0.2$ and $R^d = 0.2, R^2 = 1.0$. The results are presented respectively in Table VI and Table VII.

TABLE VI: COMPARISON OF TWO SCUC SOLUTIONS OBTAINED FOR $R^d = 0.2, R^w = 0.2$, EVALUATED WITH UNIFORMLY-DISTRIBUTED STRESSORS

R^d	R^w	Save (k$)	Cost red. (%)	Consr. cost (k$)	Deter. std (k$)	RA. std (k$)
0.1	0.2	-0.09	0.00	2.69	0.62	0.62
0.1	0.6	-0.09	0.00	2.61	0.52	0.52
0.1	1.0	0.06	0.00	2.60	0.90	0.59
0.1	1.4	0.33	0.01	2.70	1.38	0.78
0.2	0.2	0.61	0.01	5.59	2.55	1.22
0.2	0.6	1.65	0.03	6.19	4.23	2.23
0.2	1.0	2.68	0.05	7.58	6.28	3.95
0.2	1.4	2.30	0.04	8.23	6.50	4.95
0.3	0.2	6.11	0.11	19.62	15.17	12.89
0.3	0.6	6.50	0.12	20.53	12.85	11.71
0.3	1.0	6.13	0.11	21.87	14.51	11.34
0.3	1.4	5.45	0.10	22.45	12.09	10.68

TABLE VII: COMPARISON OF TWO SCUC SOLUTIONS OBTAINED FOR $R^d = 0.2, R^w = 1.0$, EVALUATED WITH UNIFORMLY-DISTRIBUTED STRESSORS

R^d	R^w	Save (k$)	Cost red. (%)	Consr. cost (k$)	Deter. std (k$)	RA. std (k$)
0.1	0.2	-0.88	-0.02	2.52	0.62	0.59
0.1	0.6	-0.88	-0.02	2.44	0.52	0.50
0.1	1.0	-0.74	-0.01	2.45	0.90	0.57
0.1	1.4	-0.36	-0.01	2.44	1.38	0.58
0.2	0.2	0.08	0.00	5.15	2.55	1.19
0.2	0.6	1.65	0.03	5.23	4.23	1.19
0.2	1.0	4.03	0.07	5.28	6.28	1.51
0.2	1.4	4.34	0.08	5.23	6.50	1.60
0.3	0.2	16.66	0.31	8.11	15.17	2.05
0.3	0.6	17.60	0.33	8.48	12.85	2.21
0.3	1.0	16.69	0.31	10.35	14.51	4.76
0.3	1.4	15.79	0.29	11.16	12.09	6.14

Even with less adverse realizations, the risk-aware dispatch solutions still save costs at higher variation levels. The standard deviation of total costs is also smaller under risk-aware solutions, indicating a more reliable dispatch schedule. Due to the dispatch of additional capacity, the risk-aware solution is more costly at very low variation levels, yet such cost is relatively small compared with potential savings when there are higher variations.

V. CONCLUSION

In this work, we enhance the SCUC computation to better handle load and wind generation volatility, which reduces the consumer cost due to real-time price spike. Our method features a data-driven PCA-based uncertainty set, which models

the locational correlation in uncertain data. We develop cutting planes and heuristics to solve the non-convex optimization model efficiently. Validated through the extensive case study on an NYISO dataset, our approach effectively reduces total costs and cost volatility under adverse scenarios. Notably, these benefits are observed across various levels of variation, and are achieved without substantial expenses for dispatch.

APPENDIX

A. Example: Binding Ramping Constraint and LMP

We provide an example to demonstrate that when $\mathbf{y}$ changes to $\mathbf{y}'$ and when a ramping constraint is binding, it is possible that the LMP at hour $\hat{t}$ decreases even if $\mathcal{I}_{0\hat{t}} \subseteq \mathcal{I}'_{0\hat{t}}$, i.e., all generators were off under $\mathbf{y}$ remain off when switching to $\mathbf{y}'$.

Consider a system with uncongested network, three thermal generators $g \in \{1,2,3\}$ and two hours $t \in \{1,2\}$. Let the real-time load be 59 for both hours and $P_g^{\min}$ equals 0 for all generators. Also, let the generator capacity $\mathbf{P}^{\max} = [50, 10, 50]$ and real-time ramping limit $\mathbf{M}^{\mathrm{RT}} = [\infty, \infty, 1]$. Assume that all generators have no startup or shutdown cost and that they have constant cost for each MWh of power output, which equals 1, 2, and 3 respectively for the three generators. Initially, let all generators be committed in both hours, i.e., $\mathcal{I}_{0t} = \emptyset, \forall t \in \{1,2\}$. Then the vector of optimal production decisions (p_{gt}) is $\mathbf{p} = [50, 9, 0; 50, 9, 0]$ and the LMP $\boldsymbol{\lambda} = [2, 2]$.

Now we switch from $\mathbf{y}$ to $\mathbf{y}'$ by turning off $g = 1$ at hour $t = 1$. Then the updated production decisions $\mathbf{p}' = [0, 10, 49; 11, 0, 48]$. Note that $p'_{32} = 48$ because the ramping limit of generator 3 is 1. Since generator 1 has no ramping limit and $p'_{12} \in (0, 50)$, it is the marginal generator and sets the LMP in hour 2 and thus $\lambda'_2 = 1$. Therefore, the LMP at $t = 2$ decreases even if $\mathcal{I}_{02} \subseteq \mathcal{I}'_{02} = \emptyset$.

REFERENCES

[1] Y. M. Al-Abdullah, M. Abdi-Khorsand, and K. W. Hedman, "The role of out-of-market corrections in day-ahead scheduling," *IEEE Trans. Power Syst.*, vol. 30, no. 4, pp. 1937–1946, 2014.

[2] U. Helman, B. F. Hobbs, and R. P. O'Neil, "The design of us wholesale energy and ancillary service auction markets: Theory and practice," in *Competitive Electricity Markets*. Elsevier, 2008, pp. 179–243.

[3] NYISO, "NYISO day-ahead scheduling manual," *NYISO Energy Market Operations*, December 2022.

[4] J. Zarnikau, C.-K. Woo, C. Gillett, T. Ho, S. Zhu, and E. Leung, "Day-ahead forward premiums in the texas electricity market," *J. Energy Mark.*, vol. 8, pp. 1–20, 2015.

[5] ISO New England, "2022 annual markets report," ISO New England, Tech. Rep., June 2023. [Online]. Available: https://www.iso-ne.com/static-assets/documents/2023/06/2022-annual-markets-report.pdf

[6] CAISO, "Caiso open access same-time information system," 2023, accessed: 2023-11-16. [Online]. Available: http://oasis.caiso.com/mrioasis/logon.do

[7] A. Jha and F. A. Wolak, "Testing for market efficiency with transactions costs: An application to convergence bidding in wholesale electricity markets," in *Industrial Organization Seminar, Yale University*, 2013.

[8] Q. P. Zheng, J. Wang, and A. L. Liu, "Stochastic optimization for unit commitmenta review," vol. 30, no. 4, pp. 1913–1924, 2014.

[9] L. A. Roald, D. Pozo, A. Papavasiliou, D. K. Molzahn, J. Kazempour, and A. Conejo, "Power systems optimization under uncertainty: A review of methods and applications," *Electr. Power Syst. Res.*, vol. 214, p. 108725, 2023.

[10] S. Takriti, J. R. Birge, and E. Long, "A stochastic model for the unit commitment problem," *IEEE Trans. Power Syst.*, vol. 11, no. 3, pp. 1497–1508, 1996.

[11] P. Carpentier, G. Gohen, J.-C. Culioli, and A. Renaud, "Stochastic optimization of unit commitment: a new decomposition framework," *IEEE Trans. Power Syst.*, vol. 11, no. 2, pp. 1067–1073, 1996.

[12] J. M. Morales, A. J. Conejo, and J. Pérez-Ruiz, "Economic valuation of reserves in power systems with high penetration of wind power," *IEEE Trans. Power Syst.*, vol. 24, no. 2, pp. 900–910, 2009.

[13] L. Wu, M. Shahidehpour, and T. Li, "Stochastic security-constrained unit commitment," *IEEE Trans. Power Syst.*, vol. 22, no. 2, pp. 800–811, 2007.

[14] Y. Dvorkin, H. Pandžić, M. A. Ortega-Vazquez, and D. S. Kirschen, "A hybrid stochastic/interval approach to transmission-constrained unit commitment," *IEEE Trans. Power Syst.*, vol. 30, no. 2, pp. 621–631, 2014.

[15] B. Wang and B. F. Hobbs, "Real-time markets for flexiramp: A stochastic unit commitment-based analysis," *IEEE Trans. Power Syst.*, vol. 31, no. 2, pp. 846–860, 2015.

[16] K. Sundar, H. Nagarajan, M. Lubin, L. Roald, S. Misra, R. Bent, and D. Bienstock, "Unit commitment with n-1 security and wind uncertainty," in *Power Syst. Comput. Conf.* IEEE, 2016, pp. 1–7.

[17] R. Jiang, J. Wang, and Y. Guan, "Robust unit commitment with wind power and pumped storage hydro," *IEEE Trans. Power Syst.*, vol. 27, no. 2, pp. 800–810, 2011.

[18] D. Bertsimas, E. Litvinov, X. A. Sun, J. Zhao, and T. Zheng, "Adaptive robust optimization for the security constrained unit commitment problem," *IEEE Trans. Power Syst.*, vol. 28, no. 1, pp. 52–63, 2012.

[19] D. Bertsimas and M. Sim, "The price of robustness," *Oper. Res.*, vol. 52, no. 1, pp. 35–53, 2004.

[20] F. Golestaneh, P. Pinson, and H. B. Gooi, "Polyhedral predictive regions for power system applications," *IEEE Trans. Power Syst.*, vol. 34, no. 1, pp. 693–704, 2018.

[21] N. Zhao and F. You, "Sustainable power systems operations under renewable energy induced disjunctive uncertainties via machine learning-based robust optimization," *Renew. Sustain. Energy Rev.*, vol. 161, p. 112428, 2022.

[22] M. B. Haugh and O. R. Lacedelli, "Scenario analysis for derivative portfolios via dynamic factor models," *Quant. Fin.*, vol. 20, no. 4, pp. 547–571, 2020.

[23] S. Wold, K. Esbensen, and P. Geladi, "Principal component analysis," *Chemom. Intell. Lab. Sys.*, vol. 2, no. 1-3, pp. 37–52, 1987.

[24] C. Ning and F. You, "Data-driven decision making under uncertainty integrating robust optimization with principal component analysis and kernel smoothing methods," *Comput. Chem. Eng.*, vol. 112, pp. 190–210, 2018.

[25] H. M. Markowitz, "Portfolio selection," *The Journal of Finance*, vol. 1, pp. 71–91, 1952.

[26] J. Benders, "Partitioning procedures for solving mixed-variables programming problems," *Numerische Mathematik*, vol. 4, no. 1, pp. 238–252, 1962.

[27] L. A. Wolsey, *Integer programming*. John Wiley & Sons, 2020.

[28] G. Laporte and F. V. Louveaux, "The integer l-shaped method for stochastic integer programs with complete recourse," *Oper. Res. Lett.*, vol. 13, no. 3, pp. 133–142, 1993.

[29] J. N. Hooker and G. Ottosson, "Logic-based benders decomposition," *Math. Program.*, vol. 96, no. 1, pp. 33–60, 2003.

[30] R. Mieth, Y. Dvorkin, and M. A. Ortega-Vazquez, "Risk-aware dimensioning and procurement of contingency reserve," *IEEE Trans. Power Syst.*, vol. 38, no. 2, pp. 1081–1093, 2022.

[31] EIA, "Short-term energy outlook supplement: Sources of price volatility in the ERCOT market," 2022. [Online]. Available: https://www.eia.gov/outlooks/steo/special/supplements/2022/2022_sp_03.pdf

[32] ISO New England, "FAQs: Locational marginal pricing," https://www.iso-ne.com/participate/support/faq/lmp, 2023, accessed: 2023-11-07.

[33] Y. Dvorkin, R. Fernandez-Blanco, D. S. Kirschen, H. Pandžić, J.-P. Watson, and C. A. Silva-Monroy, "Ensuring profitability of energy storage," *IEEE Trans. Power Syst.*, vol. 32, no. 1, pp. 611–623, 2017.

[34] Z. Liang, R. Mieth, Y. Dvorkin, and M. A. Ortega-Vazquez, "Weather-driven flexibility reserve procurement," *arXiv preprint arXiv:2209.00707*, 2022.

[35] Y. Jiang, T. Richards, and B. Richards, "Nogood backmarking with min-conflict repair in constraint satisfaction and optimization," in *Principles and Practice of Constraint Programming: Second International Workshop, PPCP'94 Rosario, Orcas Island, WA, USA, May 2–4, 1994 Proceedings*. Springer, 1994, pp. 21–39.

[36] National Renewable Energy Laboratory (NREL), "Wind Integration National Dataset (WIND) Toolkit." [Online]. Available: https://www.nrel.gov/grid/wind-toolkit.html

[37] NYISO, "Energy market & operational data." [Online]. Available: https://www.nyiso.com/energy-market-operational-data